Progress in Organic Coatings 89 (2015) 150–159

Contents lists available at ScienceDirect

Progress in Organic Coatings

journal homepage: www.elsevier.com/locate/porgcoat

Formation of icephobic film from POSS-containing fluorosilicone multi-block methacrylate copolymers

Xiaohui Li [a], Kaiqiang Zhang [a], Yunhui Zhao [a], Kongying Zhu [b], Xiaoyan Yuan [a,*]

[a] School of Materials Science and Engineering, and Tianjin Key Laboratory of Composite and Functional Materials, Tianjin University, Tianjin 300072, China
[b] Analysis and Measurement Center, Tianjin University, Tianjin 300072, China

ARTICLE INFO

Article history:
Received 28 February 2015
Received in revised form 25 August 2015
Accepted 27 August 2015

Keywords:
Fluorosilicone copolymers
Multi-block
Polyhedral oligomeric silsesquioxane
Synergistic effect
Icephobicity

ABSTRACT

Polyhedral oligomeric silsesquioxane (POSS)-containing fluorosilicone multi-block methacrylate copolymers (PDMS-*b*-(PMAPOSS-*b*-PFMA)$_2$) were synthesized *via* RAFT polymerization of methacryloisobutyl POSS (MAPOSS) with hexafluorobutyl methacrylate (HFBMA) or dodecafluoroheptyl methacrylate (DFHMA) as different fluorinated side groups. A macro-RAFT chain transfer agent of polydimethylsiloxane with dithiobenzoate groups at both ends was initially used. Characterizations of surface chemical composition and morphology of the copolymer films suggested that the PDFHMA chains with longer fluorinated side groups, as compared with PHFBMA chains, were easy to migrate onto the surface and the surface roughness was enhanced by introducing PMAPOSS segments. The film of multi-block copolymer PDMS-*b*-(PMAPOSS-*b*-PDFHMA)$_2$ produced a fluorine-rich surface due to the enrichment of fluorinated blocks and exhibited the highest receding contact angle ($103.8 \pm 0.5^\circ$) and lowest water contact angle hysteresis ($8.7 \pm 1.4^\circ$) among all the samples, attributed to the introduction of PMAPOSS segments and the synergistic effect of silicon and fluorine. Measurements of icephobic properties demonstrated that the supercooled water droplet could easily slip away from the tilted PDMS-*b*-(PMAPOSS-*b*-PDFHMA)$_2$ surface (45°) at $-20\,^\circ$C and the ice shear strength tended to decrease from 361 kPa to 264 kPa with incorporation of PMAPOSS blocks in comparison with PDMS-*b*-(PFMA)$_2$. However, it was found that decreasing wettability of the block copolymer film did not have significant effect on reducing the ice shear strength. The prepared POSS-containing fluorosilicone multi-block methacrylate copolymers with good icephobicity can be used as icephobic coating materials potentially.

1. Introduction

Ice accumulation on exposed surfaces such as aircrafts, wind turbines, and power lines may result in severe accidents and large economic losses [1,2]. In the past few years, a considerable amount of researches have been conducted on the development of icephobic materials [3–6]. Low surface energy materials, including silicone-based polymers and fluoropolymers, are often applied to prepare hydrophobic surfaces, which can be used as icephobic materials. It is well known that the interaction between the substance and ice includes electrostatic forces, hydrogen bonding, van der Waals forces and mechanical interlocking. Because of flexibility of polydimethylsiloxane (PDMS) chains at low temperature, the PDMS-based polymer can prevent mechanical interaction and reduce ice adhesion strength, which makes it a good candidate for icephobic coatings [7,8]. Fluoropolymers may also be used as icephobic materials due to their low dielectric constant, which can reduce the electrostatic force between the substrate and ice, and result in low ice adhesion strength [9]. However, both PDMS-based polymers and fluoropolymers have drawbacks in actual icephobic coating applications. The former shows poor mechanical properties and low oil repellency, while the latter usually has a higher T_g value.

Recently, increasing attention has been attracted to incorporation of fluorinated polymeric components into PDMS-based polymers to obtain fluorosilicone copolymers. Fluorosilicone copolymers combining the advantages of fluoropolymer and silicone, can possibly surmount their individual weakness and thus may be used as ice or snow repellent coatings [10–13]. Meanwhile, for a heterogeneous polymer surface containing both fluorocarbon and siloxane, the interaction energies between the polymer surface and water would be decreased when both fluorocarbon group and siloxane group close into a water molecule. Thus, the synergistic

* Corresponding author.
E-mail addresses: yuanxy@tju.edu.cn, xyuan28@yahoo.com (X. Yuan).

http://dx.doi.org/10.1016/j.porgcoat.2015.08.018
0300-9440/

effect of silicon and fluorine would contribute to the reduction of contact angle hysteresis [14,15].

The surface morphology would have great influence on the icephobicity of the materials. Compared with micron scale roughness surfaces, the nanoscaled surfaces would possible possess better icephobic behaviors [7,16–18]. Polyhedral oligomeric silsesquioxane (POSS) has a cage-like inorganic core in the range of 1–3 nm, covalently surrounded by organic corner groups, which endow the POSS molecule with a higher solubility in organic solvents and can be used to modify the properties of polymers at the molecular level [19,20]. The incorporation of POSS units into polymer may improve the properties such as mechanical strength, hydrophobicity and thermostability, and can also increase the surface roughness of polymers [21–23].

Because of compatibility with a wide range of functional monomers and ability to control polymer architecture and molecular weight [24], reversible addition–fragmentation chain transfer (RAFT) polymerization is adopted in the study to synthesize POSS-containing fluorosilicone copolymer with well-defined structure, which allows greater insight into the structure–icephobicity relationship.

In the previous reports, we attempted to synthesize fluorosilicone block copolymers *via* free radical polymerization and RAFT polymerization [25,26]. The icephobicity results showed that the fluorosilicone block copolymer surfaces could decrease ice adhesion strength indeed, but the water droplet could hardly slide off the copolymer surfaces. It was reported that rapid de-wetting surface can be achieved by increasing receding contact angle or by removing water droplets through minimization of contact angle hysteresis [27,28]. In order to improve the icephobicity of the fluorosilicone block copolymer, in this study, a macro-RAFT chain transfer agent of polydimethylsiloxane with dithiobenzoate groups at both ends (CTA-PDMS-CTA) was initially used for RAFT polymerization of methacryloisobutyl POSS (MAPOSS) with hexafluorobutyl methacrylate (HFBMA) or dodecafluoroheptyl methacrylate (DFHMA) as the fluorinated methacrylate (FMA) monomers. The effect of different fluorinated side groups and PMAPOSS segments in the prepared POSS-containing fluorosilicone multi-block methacrylate copolymers (PDMS-*b*-(PMAPOSS-*b*-PFMA)$_2$) on the wettability and icephobic properties of copolymer films were investigated. PFMA with low surface energy was architected as the end block for facilitating fluorinated groups to migrate onto the surface. PMAPOSS was introduced for improving hydrophobicity and modifying the surface morphology of the copolymer film. The relationship between the wettability and the icephobic properties was also investigated. It was hypothesized that this specific integration of PMAPOSS block and enrichment of fluorinated groups on the copolymer surface could enhance the hydrophobic and icephobic properties.

2. Experimental methods

2.1. Materials

α,ω-Dihydrogen-terminated poly(dimethylsiloxane) (H-PDMS-H, 10,000 g/mol) was supplied by Hangzhou Silong Chem-Tech, Hangzhou, China. MAPOSS was purchased from Hybrid Plastics, USA, and used as received. HFBMA and DFHMA were supplied by Xeogia Fluorin-Silicon Chemical Co. Ltd., China, and purified by passing over a column of alumina to remove inhibitor. *N,N′*-Dicyclohexylcarbodiimide (DCC) and 4-dimethylaminopyridine (DMAP) were purchased from Sigma–Aldrich. 2,2′-Azobisisobutyrobutyl acrylate (AIBN) was obtained from Tianjin Kemiou Chemical Reagent Co. Ltd., China, and used after recrystallization by ethanol. α,α,α-Trifluorotoluene (TFT) was purchased from Tianjin Heowns Biochem Technologies LLC, Tianjin, China. All other reagents were supplied by Tianjin Kermel Reagent Co. Ltd, China, and used without further purification.

2.2. Synthesis

The POSS-containing fluorosilicone multi-block methacrylate copolymers were synthesized by RAFT polymerization (Scheme 1). The detailed compositions of the prepared copolymers are shown in Table 1.

CTA-PDMS-CTA was prepared by the DCC/DMAP catalyzed esterification of 4-cyanopentanoic acid dithiobenzoate (CPADB) with hydroxyl-terminated PDMS (HO-PDMS-OH), whereas CPADB and HO-PDMS-OH were synthesized according to the references [29,30]. Typically, HO-PDMS-OH (10 g, 1 mmol), CPADB (0.837 g, 3 mmol), DCC (0.931 g, 4 mmol) and DMAP (0.116 g, 0.9 mmol) were charged into a 150 mL flask with 50 mL of anhydrous CH_2Cl_2. The reaction mixture was stirred under N_2 protection for 12 h at 0 °C, and then for 20 h at room temperature. The precipitated dicyclohexylurea was filtered off. The crude product was precipitated in methanol for three times and dried under vacuum for 24 h. CTA-PDMS-CTA was obtained as red oil-like liquid.

The synthesized CTA-PDMS-CTA was used as macro-RAFT chain transfer agent to synthesize a PDMS-*b*-(PMAPOSS)$_2$ triblock copolymer *via* RAFT polymerization. In a typical experiment, CTA-PDMS-CTA (0.6 g, 0.05 mmol), MAPOSS (1.028 g, 1.09 mmol) and AIBN (3.6 mg, 0.022 mmol) were dissolved in 1.8 mL of toluene and placed in a 50 mL round-bottom. Then, argon gas was passed through the solution for 30 min to eliminate oxygen. The bottle was immersed in a water bath at 70 °C and the polymerization was carried out for 10 h under argon atmosphere. Pure PDMS-*b*-(PMAPOSS)$_2$ was obtained from precipitation in methanol. The product designated as **S-POSS** was then dried in a vacuum oven overnight for further uses.

Table 1
Composition and molecular weight of the prepared fluorosilicone multi-block copolymers.

Sample	Structure	[M]:[Macro-CTA]:[I]	$\tilde{M}_{n,NMR}$ (×10^4)	$\tilde{M}_{n,GPC}$ (×10^4)	DP_n [a] (MAPOSS)	DP_n [a] (FMA)	W_F [b] (wt%)	PDI[c]
–	CTA-PDMS-CTA	–	–	1.06	–	–	–	1.28
S-POSS	PDMS-*b*-(PMAPOSS)$_2$	20:1:0.4	2.10	2.03	11	–	–	1.15
S-6F	PDMS-*b*-(PHFBMA)$_2$	50:1:0.4	1.93	1.51	–	35	0.20	1.18
S-POSS-6F	PDMS-*b*-(PMAPOSS-*b*-PHFBMA)$_2$	100:1:0.4	3.45	2.51	11	54	0.17	1.24
S-12F	PDMS-*b*-(PDFHMA)$_2$	50:1:0.4	2.26	1.81	–	30	0.29	1.09
S-POSS-12F	PDMS-*b*-(PMAPOSS-*b*-PDFHMA)$_2$	50:1:0.4	3.46	2.37	11	34	0.21	1.18

[a] Measured by ^{1}H NMR.
[b] W_F = FMA conversion × F%, F% represents F element content in FMA.
[c] Obtained from GPC.

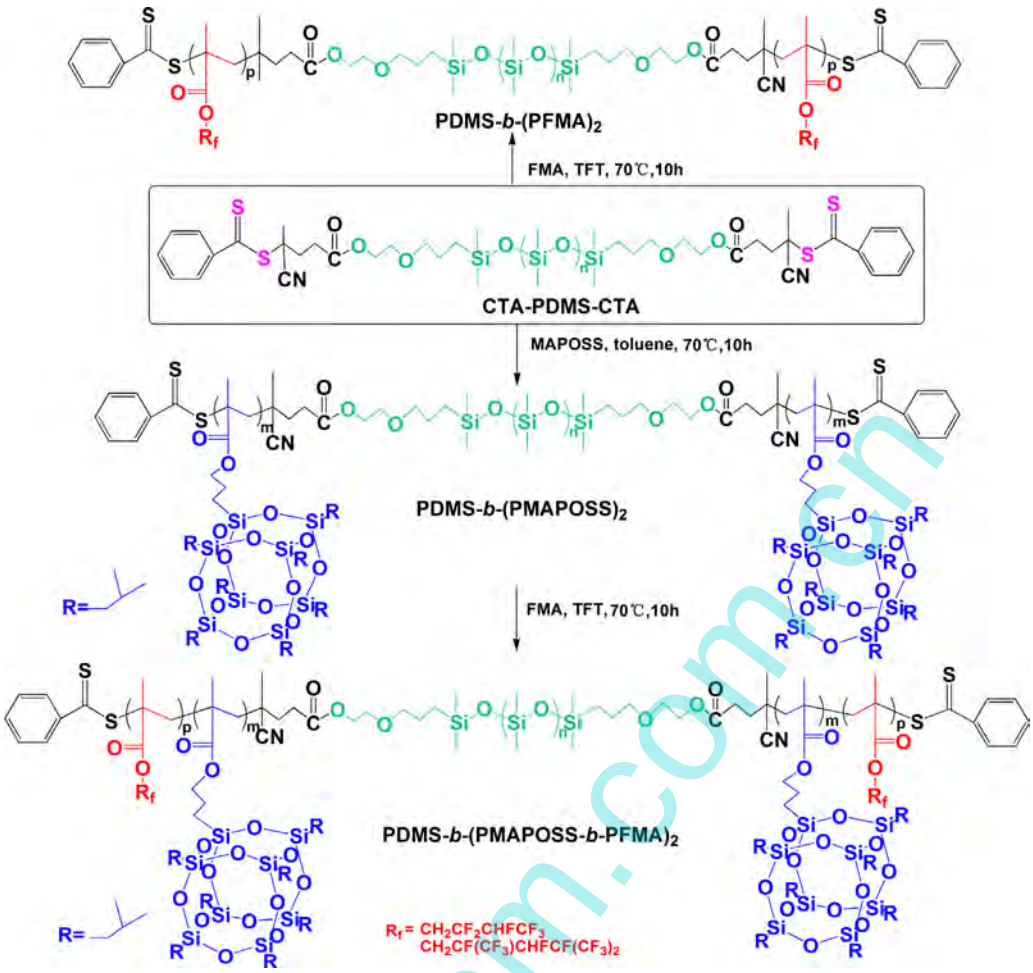

Scheme 1. Synthesis of PDMS-*b*-(PMAPOSS)$_2$, PDMS-*b*-(PFMA)$_2$ and PDMS-*b*-(PMAPOSS-*b*-PFMA)$_2$ *via* RAFT polymerization.

The pentablock copolymer PDMS-*b*-(PMAPOSS-*b*-PFMA)$_2$ was prepared by PDMS-*b*-(PMAPOSS)$_2$ and FMA (HFBMA or DFHMA). Typically, PDMS-*b*-(PMAPOSS)$_2$ (0.8 g, 0.04 mmol), FMA [HFBMA (0.95 g, 3.8 mmol) or DFHMA (0.76 g, 1.9 mmol)] and AIBN (2.6 mg, 0.016 mmol) were dissolved in 1.8 mL of TFT and placed in a 50 mL round-bottom. Then, argon gas was passed through the solution for 30 min to eliminate oxygen. The bottle was subsequently placed in a water bath at 70 °C for 10 h and stirred under argon atmosphere. After polymerization, the block copolymer was precipitated into methanol and dried under vacuum. The products are designated as **S-POSS-6F** and **S-POSS-12F** for PDMS-*b*-(PMAPOSS-*b*-PHFBMA)$_2$ and PDMS-*b*-(PMAPOSS-*b*-PDFHMA)$_2$, respectively.

For comparison, PDMS-*b*-(PFMA)$_2$ triblock copolymers were synthesized by using the CTA-PDMS-CTA as macro-RAFT chain transfer agent *via* RAFT polymerization. Typically, CTA-PDMS-CTA (0.6 g, 0.05 mmol), FMA [HFBMA (0.68 g, 2.7 mmol) or DFHMA (1.09 g, 2.7 mmol)] and AIBN (3.6 mg, 0.022 mmol) were reacted for 10 h at 70 °C as described above. After polymerization, the block copolymer was precipitated into methanol and dried under vacuum. The products are designated as **S-6F** and **S-12F** for PDMS-*b*-(PHFBMA)$_2$ and PDMS-*b*-(PDFHMA)$_2$, respectively.

The copolymer films were prepared by spin-coating the 20 wt% copolymer solutions in TFT on polished aluminum plates (20 mm × 20 mm). The spinning speed was set at 600 rpm (6 s) and 3000 rpm (10 s) for the first and second steps, respectively. Samples were dried at room temperature in air to allow the solvent to evaporate completely. The thickness of the obtained copolymer films was around 0.5 μm.

2.3. Characterizations

Fourier transformed infrared spectroscopy (FT-IR) spectra of samples were recorded in a Spectrum 100 FT-IR spectrometer (Perkin-Elmer, USA) in the range from 4000 cm^{-1} to 500 cm^{-1} using KBr pellet technique. Proton-nuclear magnetic resonance (^{1}H NMR) analysis was carried out in Varian machines (INOVA 500 MHz and Infinity plus 300WB, USA) by dissolving the samples in deuteriochloroform.

The average relative molar mass and its distribution were determined in gel permeation chromatography (GPC, TDA305, Malvern Instruments Ltd., UK) calibrated by a polystyrene standard. THF was used as the eluent at a flow rate of 1.0 mL/min at 40 °C. Differential scanning calorimetry (DSC) was measured with a Diamond differential scanning calorimeter (NETZSCH DSC 200 F3 differential scanning calorimeter, Germany) under N_2 atmosphere at a heating rate of 10 °C min^{-1} from −150 °C to 250 °C.

Bulk copolymer morphologies were viewed under a transmission electron microscope (TEM) (Tecnai G2 F20 200 kV, The Netherlands). Samples for TEM observation were prepared by directly dropping of a drop of 1 wt% copolymer solution in TFT on the carbon-coated copper grids.

Atomic force microscope (AFM) images were obtained using tapping mode at room temperature on a CSPM5500A of Being Nano-Instruments Ltd., Guangzhou, China, equipped with E-type vertical engage piezoelectric scanner. Roughness was determined at different positions of the films and was average of at least five

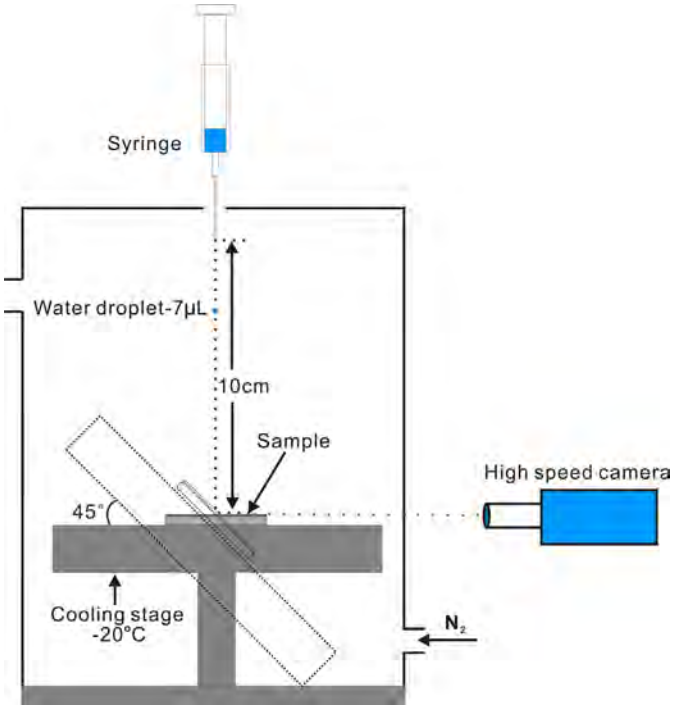

Fig. 1. Schematic diagram of water droplets dropping on the sample surface.

measurements. The thickness of the films was estimated by AFM, according to Ref. [31].

Surface composition by X-ray photoelectron spectroscopy (XPS) was investigated using a Perkin-Elmer PHI 5000C ECSAX-ray photoelectron spectroscopy in ultra-high vacuum with Al K radiation (1486.6 eV) operating at 24.2 W under a vacuum less than 5×10^{-8} Torr at 45°. The tested area was a circle with diameter of 100 μm.

Water contact angles and contact angle hysteresis of the copolymer films were measured by an optical contact angle meter (JC2000D, Shanghai Zhongchen Equipment Ltd., China) at room temperature and ambient humidity. The measurement of contact angle hysteresis was carried out using 5 μL water droplets which expanded and shrunk by 10 μL at 0.1–1.0 μL/s *via* a needle from a syringe. Images of the droplets were captured by a CCD camera and analyzed to obtain the advancing and receding contact angles, and values of the water contact angle hysteresis were calculated. The surface energies of the copolymer films were evaluated by measuring the static water and hexadecane contact angles on the surface. A drop of the probe liquid (deionized water or hexadecane) in 5 μL was used. The surface energy was calculated according to the equation by Owens–Wendt–Kaelble method [32]. All the contact angles presented are average of five measurements.

The impact experiments of water droplets were conducted using the apparatus illustrated schematically in Fig. 1. The coated Al plate (20 mm × 20 mm) was placed onto the horizontal or tilted (45°) cooling stage. A syringe (50 μL) with pointy needle was fixed above coated Al plate. The distance between the needle tip and coated Al plate was 10 cm. The water was cooled in refrigerator as the source of 0 °C water. The cooling stage could be controlled at −20 °C in a transparent chamber which was purged with nitrogen to decrease the humidity. Relative humidity inside the chamber was controlled to be less than 20% by flowing of dry nitrogen during the cooling period to minimize frost formation on the samples. During the impact experiment, a water droplet (7 μL) at room temperature or 0 °C was dropped onto the sample surface. The whole impacting process was recorded using a high speed camera (Olympus i-SPEED LT 4GB Color, Japan) operated with a frame speed of 1000 frames per second (fps) and an image resolution of 800 × 600 pixels.

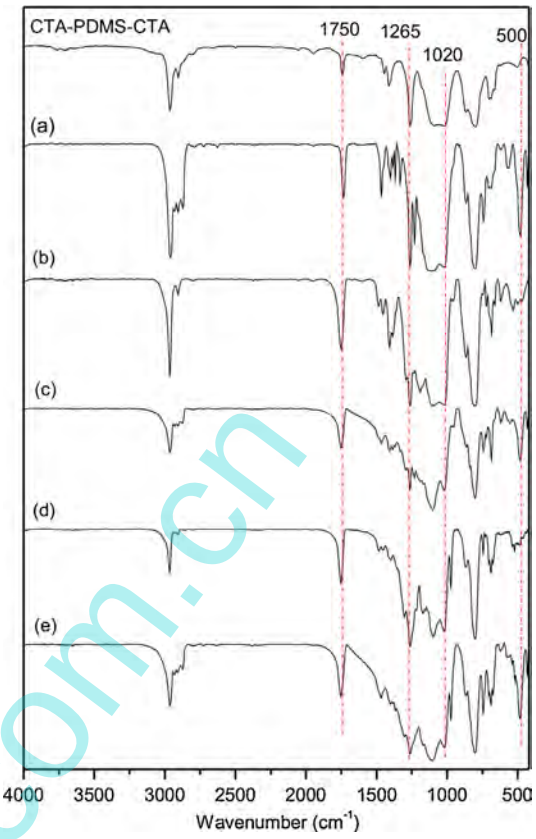

Fig. 2. FTIR spectra of CTA-PDMS-CTA and the fluorosilicone multi-block copolymers. (a) **S-POSS**, (b) **S-6F**, (c) **S-POSS-6F**, (d) **S-12F**, (e) **S-POSS-12F**.

The ice shear strength tests were performed using a custom-made cooling stage described in our previous work [25,33]. Briefly, samples, *i.e.*, the Al plate (20 mm × 20 mm) coated by the copolymers, were placed onto the cooling stage. The glass column was put on the Al plate and filled with 450 μL of fresh deionized water. The temperature of the stage reached to −15 °C at a rate of 2 °C min^{-1} and was maintained for 3 h. A force transducer (Imada ZP-500 N, Japan) was mounted on a motion stage which moved forward at a rate of 0.5 mm/s to the glass columns. The maximum force was recorded for calculating the ice shear stress by a force transducer which was mounted on a motion stage. All the presented values are averages of at least eight or nine measurements for each specimen.

3. Results and discussion

The RAFT polymerization of MAPOSS and FMA was carried out by using CTA-PDMS-CTA. It was assumed that the introduction of PMAPOSS and enrichment of fluorinated groups on the copolymer surface could improve the hydrophobic and icephobic properties. The microphase-separated structure, surface chemical composition and icephobic properties of the prepared block copolymer films were investigated in the following sections.

3.1. Synthesis of POSS-containing fluorosilicone block copolymers

Fig. 2 shows the FT-IR spectra of CTA-PDMS-CTA and the block copolymers. The appearance of peak at 1750 cm^{-1} by the C=O stretching vibration in the spectrum of CTA-PDMS-CTA indicated successful synthesis of PDMS macro-RAFT chain transfer agent. The absorbances at 1265 cm^{-1} and 1020 cm^{-1} were attributed to the

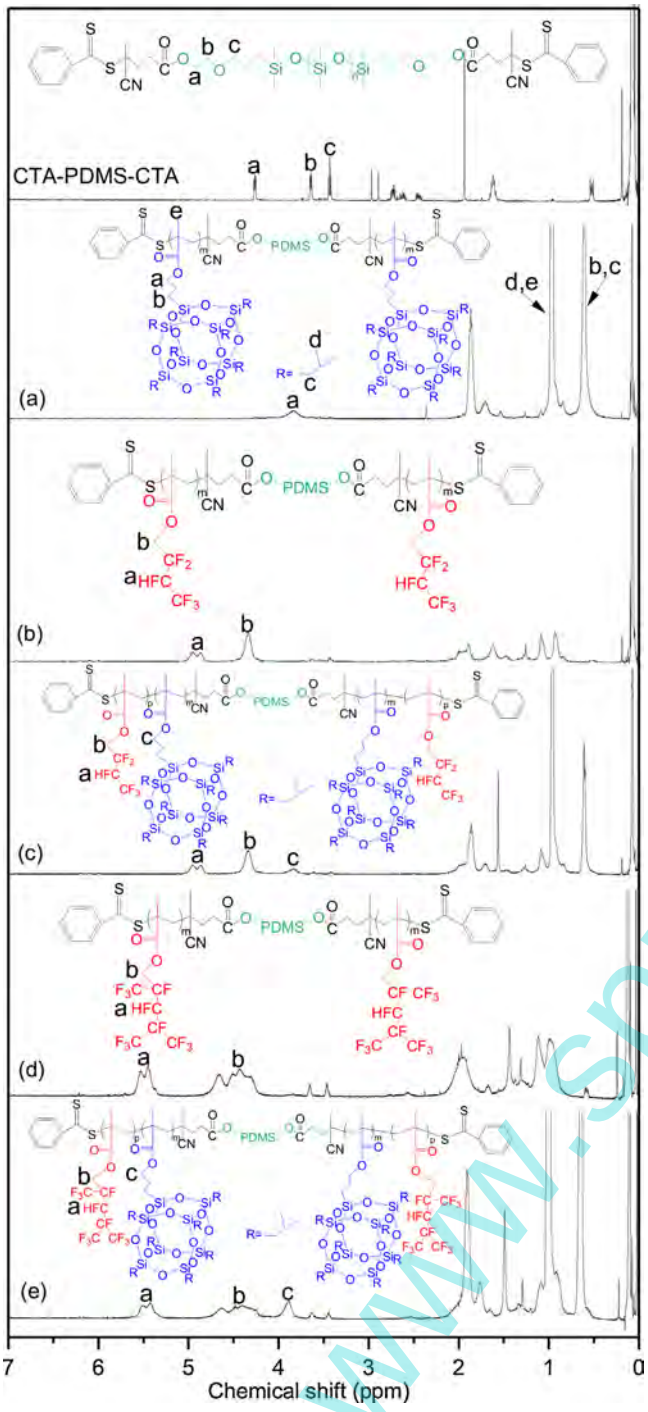

Fig. 3. ^{1}H NMR spectra of CTA-PDMS-CTA and the fluorosilicone multi-block copolymers. (a) **S-POSS**, (b) **S-6F**, (c) **S-POSS-6F**, (d) **S-12F**, (e) **S-POSS-12F**.

Si—CH_3 stretching vibration and Si—O—Si asymmetric stretching vibration, respectively, which were characteristic signals of PDMS. The absorbance at 500 cm^{-1} detected in the spectra of **S-POSS**, **S-POSS-6F** and **S-POSS-12F** was attributed to the Si—O—Si bending vibration, suggesting that MAPOSS had been incorporated into the copolymer. The peak at 1640 cm^{-1}, which was attributed to the stretching vibration of C=C group, was not detected in the spectrum of the block copolymers, indicating that there were no more redundant monomers in the resulting copolymers.

Fig. 3 presents the ^{1}H NMR spectra of CTA-PDMS-CTA and the block copolymers. The signals of δ_H at 0.1 ppm were the contribution of methyl protons of PDMS. The typical spectra

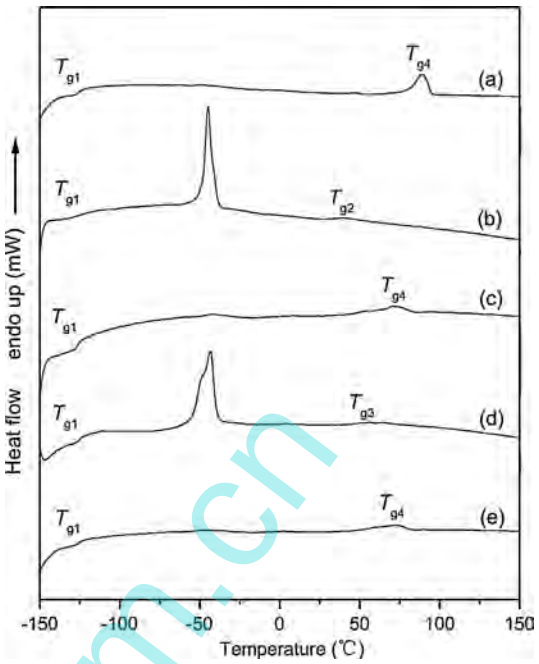

Fig. 4. DSC thermograms of the fluorosilicone multi-block copolymers. (a) **S-POSS**, (b) **S-6F**, (c) **S-POSS-6F**, (d) **S-12F**, (e) **S-POSS-12F**.

of δ_H in CTA-PDMS-CTA at 4.3 ppm, 3.6 ppm and 3.4 ppm, attributed to the $-CH_2\underline{CH_2}OCO-$, $-O-\underline{CH_2}-CH_2-O-C=O$ and $-CH_2CH_2\underline{OCH_2}-$ groups, respectively, indicated successful esterification of CPADB with HO-PDMS-OH [34]. The characteristic δ_H signals of $-\underline{CH_2}-O-C=O$ and methylene protons next to Si in PMAPOSS block were found at 3.8 ppm and 0.6 ppm correspondingly in the spectra of **S-POSS**, **S-POSS-6F** and **S-POSS-12F**. The typical δ_H in PHFBMA block were observed at 4.8–5.1 ppm and 4.3–4.6 ppm for $-\underline{CH}F$ and $-\underline{CH_2}-CF_2-$ groups correspondingly in the spectra of **S-6F** and **S-POSS-6F**. The signals of δ_H at 5.2–6.6 ppm and 4.2–4.6 ppm in the spectra of **S-12F** and **S-POSS-12F** were assigned to $-\underline{CH}F$ and $-\underline{CH_2}-CFCF_3-$ groups in PDFHMA block, respectively. The results of FT-IR and ^{1}H NMR suggested that the multi-block copolymers, including PDMS-*b*-$(PMAPOSS)_2$ (**S-POSS**), PDMS-*b*-$(PHFBMA)_2$ (**S-6F**), PDMS-*b*-(PMAPOSS-*b*-PHFBMA)$_2$ (**S-POSS-6F**), PDMS-*b*-$(PDFHMA)_2$ (**S-12F**) and PDMS-*b*-(PMAPOSS-*b*-PDFHMA)$_2$ (**S-POSS-12F**), were successfully obtained *via* RAFT polymerization.

The degree of polymerization (DP_n) of PMAPOSS, PHFBMA and PDFHMA in prepared copolymers were calculated by comparing the characteristic integral intensities of PMAPOSS (3.8 ppm), PHFBMA (4.3–4.6 ppm) and PDFHMA (5.2–6.6 ppm) with that of PDMS (0.1 ppm). The calculated values of DP_n as well as the molecular weight ($\bar{M}_{n,NMR}$, $\bar{M}_{n,GPC}$), fluorine content (W_F) and polydispersity index (PDI) of the multi-block copolymers were summarized in Table 1. It can be seen that the values of W_F of the copolymers were almost the same and the PDI were in the range of 1.09–1.24, indicating that the polymerization reactions proceed in a controlled manner.

3.2. Microphase separation

The thermal transitions of the prepared multi-block copolymers were investigated by DSC (Fig. 4). Glass transition temperature at about −125 °C (T_{g1}) attributed to the PDMS block was detected in all the copolymer thermograms. The melting peaks at about −40 °C also assigned by the PDMS block were found in sample **S-6F** and **S-12F**. As shown in Fig. 4, PHFBMA block exhibited its T_{g2} at about 40 °C in the DSC curve of **S-6F**. PDFHMA block displayed

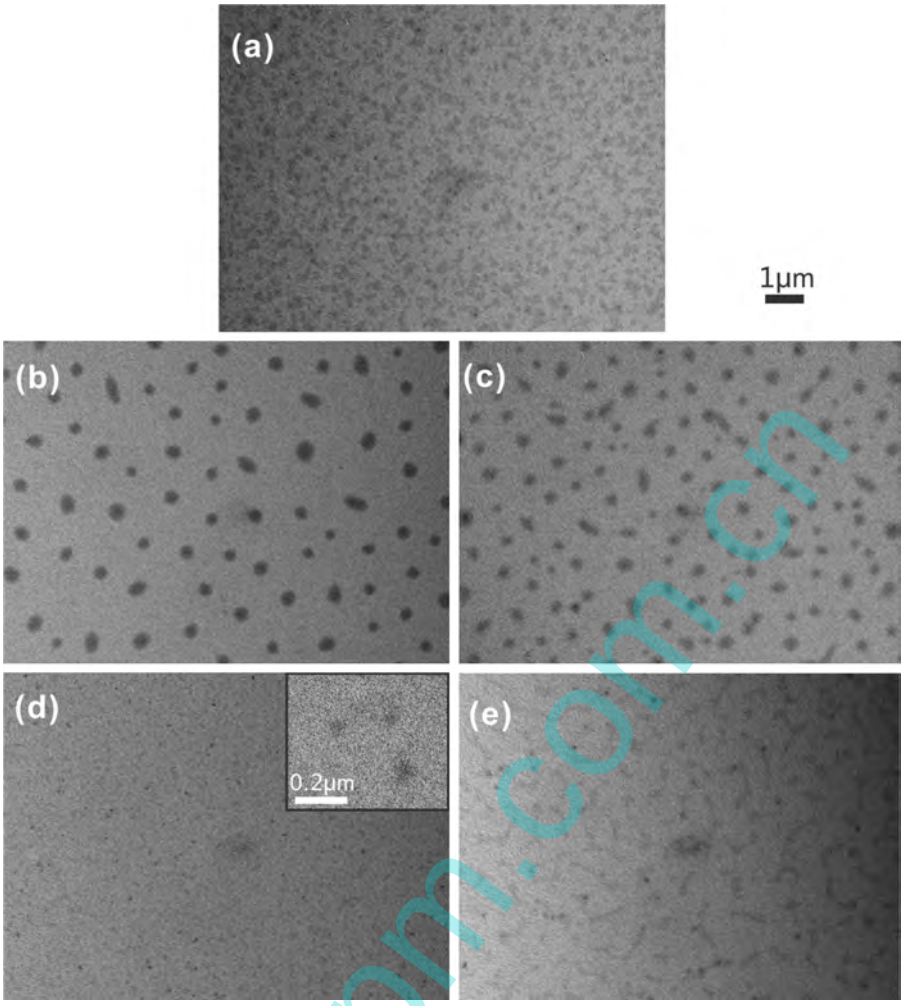

Fig. 5. TEM micrographs of the fluorosilicone multi-block copolymers. (a) **S-POSS**, (b) **S-6F**, (c) **S-POSS-6F**, (d) **S-12F**, (e) **S-POSS-12F**.

its T_{g3} at about 60 °C in **S-12F**. In addition, the glass transition at about 80 °C (T_{g4}) in **S-POSS**, **S-POSS-6F** and **S-POSS-12F** would be related with PMAPOSS. The absence of melting transitions of PDMS block in **S-POSS**, **S-POSS-6F** and **S-POSS-12F** could be associated with the POSS groups, which affected the mobility of the PDMS chains in molecular packing and therefore hindered crystallization. Because of the introduction of PMAPOSS segments, T_{g2} and T_{g3} for PHFBMA and PDFHMA were not obvious in sample **S-POSS-6F** and **S-POSS-12F**. The DSC results suggested the possibly incompatible components in the copolymers that could lead to microphase separation.

The bulk morphologies of the prepared multi-block copolymers were investigated by TEM. As the silicon element in PDMS and PMAPOSS segments has a higher electron density than the carbon atoms in PFMA, the PDMS and PMAPOSS domains appeared as dark regions, in contrast to the bright PFMA regions. Microphase separation occurs because of the thermodynamic incompatibility between the PDMS, PMAPOSS and PFMA blocks. As shown in Fig. 5, all the block copolymers exhibited microphase-separated structures with clear interfaces except for **S-POSS**, because of the similar Si—O structures in PDMS and PMAPOSS segments. The spherical aggregates with diameter approximate 200–500 nm were clearly seen in **S-6F** and **S-POSS-6F**, while small spheres with diameter approximate 40–80 nm existed in **S-12F**, and the aggregates with rod-like morphology were obtained in **S-POSS-12F**. The formation of these different aggregates could be attributed to the diverse solubility of PDMS, PMAPOSS and PFMA segments in the TFT solvent, which was insoluble for PDMS and PMAPOSS, but soluble for PFMA [35,36]. Thus the fluorosilicone block copolymers tended to self-assemble into micelle in TFT that would be made of PDMS and PMAPOSS segments as the cores and PFMA segments as the shells. The spherical microdomains in **S-6F** and **S-POSS-6F** were assignable to PDMS and PMAPOSS aggregates. Because the fluoridated side chain in PDFHMA was longer than that in PHFBMA, the interfacial free energy between the PDMS aggregate core and the solvent would decrease. Therefore, the spherical aggregates in **S-12F** and rod-like morphology in **S-POSS-12F** were found. The results of TEM confirmed the microphase separation of the block copolymers in bulk.

3.3. Surface composition and morphology

Given that the surface elemental composition has a marked impact on the surface wettability and icephobic properties of copolymer coatings [7], the surface compositions of multi-block copolymer films were evaluated by XPS (Fig. 6). The carbon, oxygen, fluorine and silicon contents as well as the F/Si ratios are summarized in Table 2. The peaks in Fig. 6 at 284.4 eV, 534.8 eV, 690.9 eV and 104.8 eV arose from C1s, O1s, F1s and Si2p core levels, respectively. It can be seen from Table 2 that all the block copolymer surfaces except for **S-POSS** contained fluorine element, but the percentages were distinct from each other. The fluorine percentages on **S-6F** (1.5 wt%) and **S-POSS-6F** (0.9 wt%) surfaces were obviously lower than those on **S-12F** (18.7 wt%) and **S-POSS-12F** (25.0 wt%)

Table 2
Element composition of the fluorosilicone multi-block copolymer film obtained by XPS and their surface roughness (R_q) analyzed by AFM.

Sample	C (atomic %)	O (atomic %)	F (atomic %)	Si (atomic %)	F/Si	R_q (nm)
S-POSS	53.5	25.4	–	21.1	–	2.77 ± 0.10
S-6F	51.6	25.3	1.5	21.6	0.07	1.34 ± 0.03
S-POSS-6F	51.7	25.4	0.9	22.0	0.04	2.36 ± 0.05
S-12F	47.0	19.8	18.7	14.5	1.29	1.96 ± 0.03
S-POSS-12F	47.5	16.8	25.0	10.7	2.34	4.05 ± 0.07

whereas the silicon percentages on the **S-6F** (21.6 wt%) and **S-POSS-6F** (22.0 wt%) were higher than those on **S-12F** (14.5 wt%) and **S-POSS-12F** (10.7 wt%), attributed to the high mobility of PDMS segments and large POSS groups hindering the migration of the PHFBMA blocks to surface. According to Ref. [36], both fluorinated segments and PDMS segments had ability to migrate onto the film surface due to the low surface energy. However, the migration of fluorinated segments was strongly limited by the competing of PDMS segments because of the flexible PDMS segments being easy to migrate onto the film surface. As shown in Table 2, **S-6F** and **S-POSS-6F** containing PHFBMA segments produced silicone-rich surfaces, while **S-12F** and **S-POSS-12F** containing PDFHMA segments produced fluorine-rich surfaces. Therefore, it could be concluded that PDFHMA segments with longer fluoridated side groups were easier to move onto the surface than PHFBMA segments. This result agrees well with previous report by Niu [36]. Table 2 shows the F/Si value of sample **S-POSS-12F** (2.34) was higher than the other samples. It could be ascribed to the introduction of the PMAPOSS block and relatively longer fluoridated side group in PDFHMA segments [36].

In addition to the surface composition, the surface morphology would also have a significant influence on the icephobic behaviors of the block copolymer films [3,4]. The surface morphologies and roughness of multi-block copolymer films were examined by AFM. In AFM height images, the low domains appear as the dark areas and the high domains correspond to the bright areas. As shown in Fig. 7, all the block copolymers demonstrated distinct microphase separation, but the morphologies were different from each other. The surface morphology of **S-POSS** film containing PDMS and PMAPOSS blocks was characterized by an irregular island type structure. However, wormlike surface structure was formed on the film surface of **S-POSS-6F**. On the other hand, the obvious honeycomb structure was observed on the film surface of **S-POSS-12F**. The surfaces **S-6F** and **S-12F** films without PMAPOSS blocks,

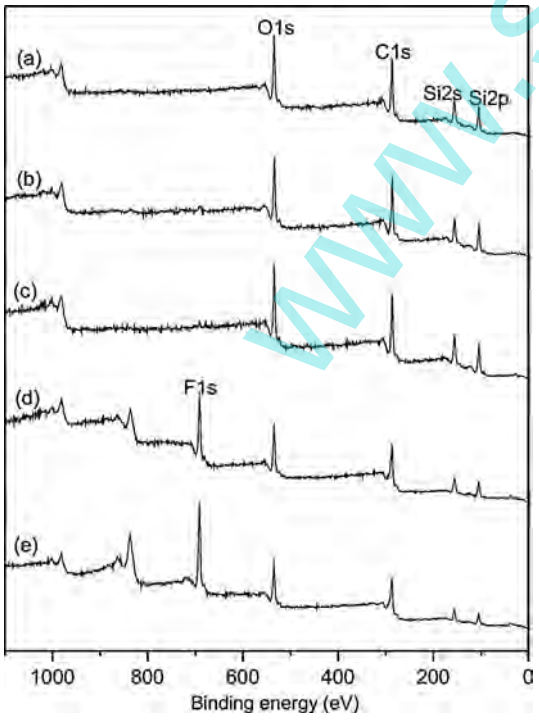

Fig. 6. Survey XPS spectra of the fluorosilicone multi-block copolymer films. (a) **S-POSS**, (b) **S-6F**, (c) **S-POSS-6F**, (d) **S-12F**, (e) **S-POSS-12F**.

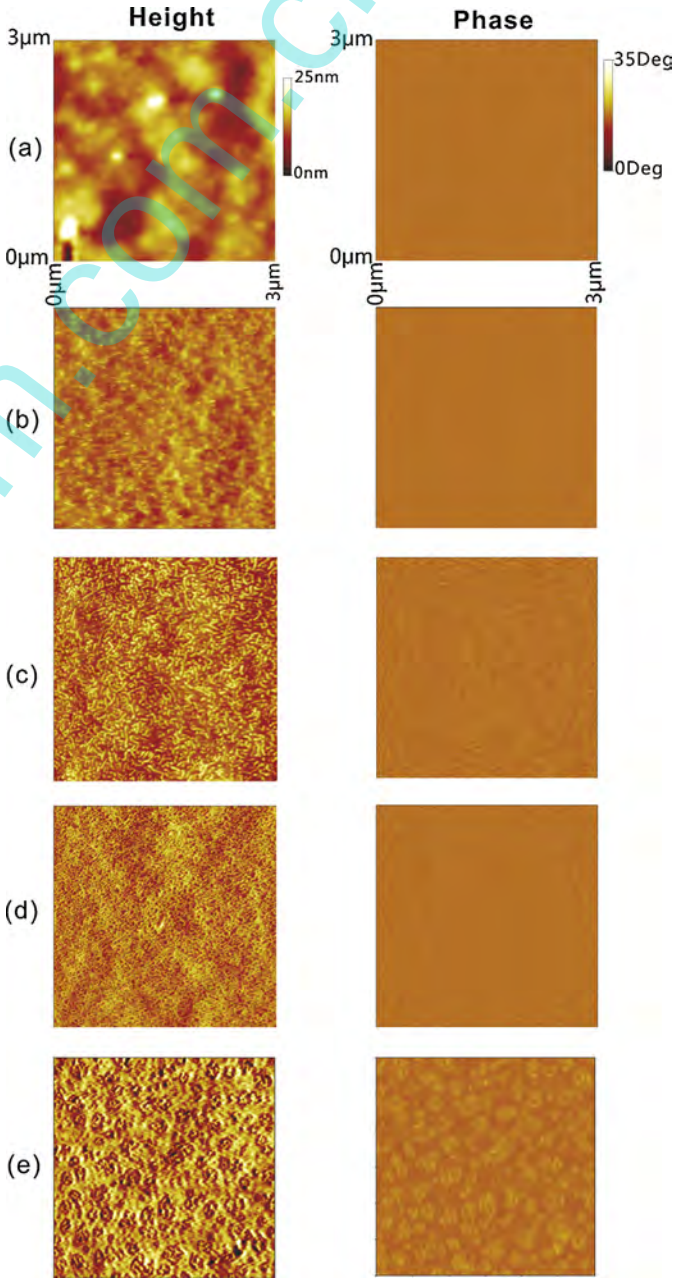

Fig. 7. AFM images of the fluorosilicone multi-block copolymer films. (a) **S-POSS**, (b) **S-6F**, (c) **S-POSS-6F**, (d) **S-12F**, (e) **S-POSS-12F**.

Table 3
Water contact angle, contact angle hysteresis and surface energy of the fluorosilicone multi-block copolymer film.

Sample	Static contact angle (°)	Advancing contact angle (°)	Receding contact angle (°)	Contact angle hysteresis (°)	Surface energy (mJ m^{-2})
S-POSS	105.5 ± 0.5	109.4 ± 1.2	91.6 ± 1.1	17.8 ± 1.7	27.04
S-6F	105.2 ± 1.0	111.7 ± 1.3	85.1 ± 1.5	26.6 ± 2.9	27.22
S-POSS-6F	106.2 ± 0.3	112.0 ± 0.6	93.6 ± 1.7	18.3 ± 2.3	26.95
S-12F	105.3 ± 0.8	112.7 ± 0.1	96.0 ± 1.3	16.7 ± 1.4	24.79
S-POSS-12F	108.2 ± 0.3	112.6 ± 1.1	103.8 ± 0.5	8.7 ± 1.4	18.42

exhibited relatively smooth nanostructures. The formation irregular island structure on **S-POSS** surface was mainly attributed to the aggregation of PMAPOSS blocks, which were likely to cluster in copolymer blocks [21]. Because TFT was a good solvent for PHFBMA, but poor solvent for PDMS and PMAPOSS [36], **S-POSS-6F** tended to self-assemble during the film formation. PDMS and PMAPOSS were easy to integrate together so as to reduce the interfacial area and form wormlike structure on **S-POSS-6F** surface. For **S-POSS-12F**, the migration of PDFHMA segments onto the film surface was easier than that of PHFBMA segments, as confirmed by XPS detection, resulting in honeycomb structure on **S-POSS-12F** surface. In the AFM phase images, microphase separation was more evidently observed for **S-POSS-6F** and **S-POSS-12F**. From Table 2, the surface roughness of **S-POSS-6F** and **S-POSS-12F** were 2.36 ± 0.05 nm and 4.05 ± 0.07 nm, respectively, which was higher than that of **S-6F** (1.34 ± 0.03 nm) and **S-12F** (1.96 ± 0.03 nm). The higher surface roughness of **S-POSS-6F** and **S-POSS-12F** could be attributed to the aggregates of PMAPOSS cages, which are more likely to cluster and migrate onto the surface of block copolymers [21,22]. The surface roughness of **S-12F** was bigger than **S-6F**, attributed to the enrichment of PDFHMA block on the film surface. Therefore, the above results indicated that the introduction of PMAPOSS could lead to higher surface roughness of films. Taking the XPS results into account, the dark areas in AFM would represent the PDMS and PHFBMA blocks, while the bright areas would show the PMAPOSS domains in **S-POSS-6F**. However, in **S-POSS-12F**, dark areas represented the PDMS blocks, and the bright areas were the PDFHMA and PMAPOSS domains.

3.4. Wettability

The water contact angles, contact angle hysteresis and surface energies of the fluorosilicone multi-block copolymer films are listed in Table 3. It can be seen that the water contact angle values of the five copolymer films were higher than 105° and the surface energy values of all the samples were less than 28 mJ m^{-2}, suggesting good hydrophobicity of all the samples. Among them, **S-POSS-12F** exhibited the highest water contact angle (108.2 ± 0.3°) as well as the lowest surface energy (18.42 mJ m^{-2}). It could be ascribed to the highest fluorine content on copolymer surface (25.0 wt%), which was confirmed by XPS detection. The contact angle hysteresis quantified as the discrepancy between the advancing and receding contact angles is an important parameter for assessing the icephobic properties depending on both the topographical structure and the chemical compositions of the copolymer surface. It can be seen from Table 3 that the advancing contact angles of the copolymer films were almost the same, but the values of receding contact angles were different. The highest value of receding contact angle (103.8 ± 0.5°) and the lowest value of contact angle hysteresis (8.7 ± 1.4°) were observed for sample **S-POSS-12F**. It could be ascribed to the large POSS groups which could prevent movement of polar groups to the surface [37] and high F/Si value of **S-POSS-12F** (2.34), as confirmed by the XPS detection. The high F/Si value could result in an enhanced synergistic effect of silicon and fluorine, that could decrease the interaction with water and contribute to the reduction of contact angle hysteresis [14,15].

3.5. Icephobic properties

3.5.1. Water impact on the copolymer surfaces

To predict the icephobic property of the POSS-containing fluorosilicone block copolymer, the impact experiment of water droplet was conducted. Fig. 8 displays the dynamic behavior of water droplets (7 μL) dropping on horizontal fluorosilicone multi-block copolymer surfaces at room temperature (or −20 °C) with 10 cm releasing height. When a water droplet was released to a solid surface, the kinetic energy of the droplet dissipated during the spreading process. If the energy dissipation was not too large, part of

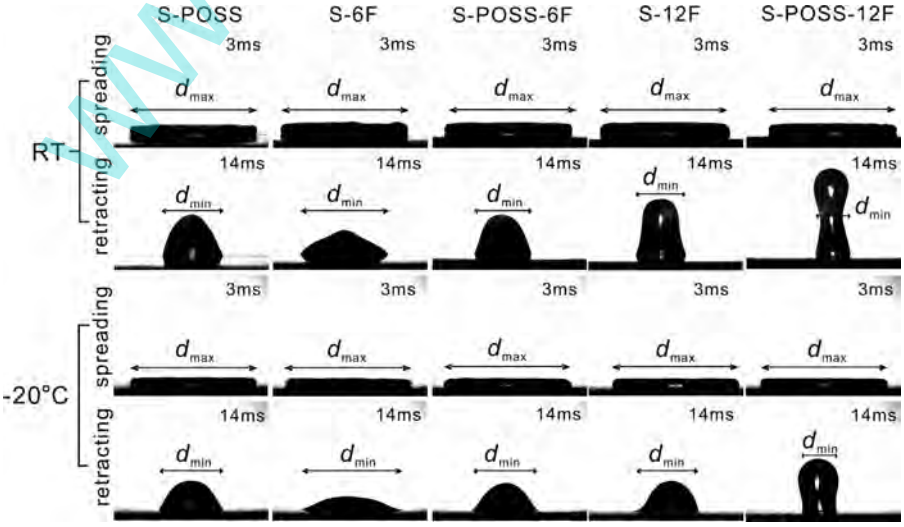

Fig. 8. Images of the dynamic behavior of 7 μL water droplets dropping on the horizontal surface of the fluorosilicone multi-block copolymers from a 10 cm height at room temperature or −20 °C.

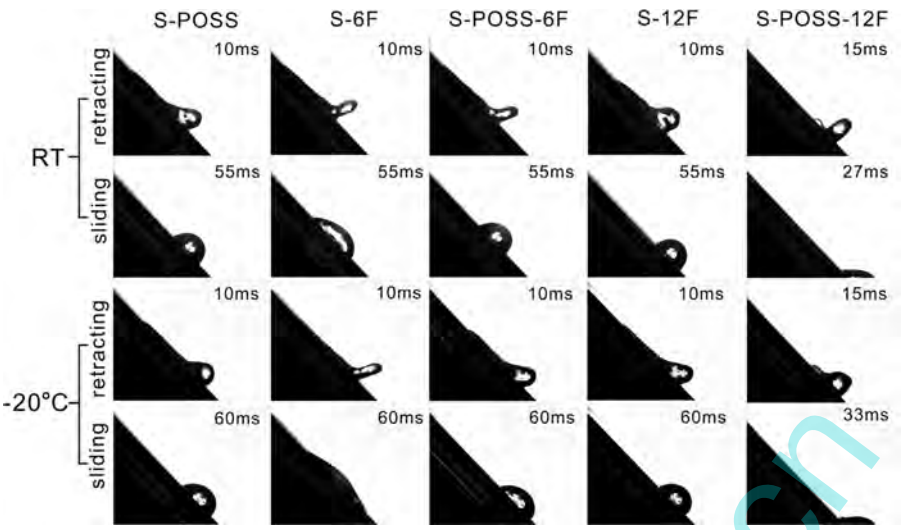

Fig. 9. Images of the dynamic behavior of 7 μL water droplets dropping on the 45°-tilted surface of the fluorosilicone multi-block copolymers from a 10 cm height at room temperature or −20 °C.

surface energy could revert to the kinetic energy and lead to retracting. The retraction process could mainly reflect the interaction between water droplet and surface [38,39]. It can be seen from Fig. 8 that the maximum spreading diameters (d_{max}) were almost the same on the five film surfaces, but the minimum retraction diameters (d_{min}) were different. The smallest d_{min} was achieved with sample **S-POSS-12F**, mainly attributed to its higher receding contact angle, as compared with other copolymer films [27,40]. The retraction of droplets is caused by the retraction force, which is a function of the apparent receding contact angle, as reported by Bahadur et al. [39]. Meanwhile, according to Ref. [41], contact angle hysteresis is one way of the energy dissipation of water droplets during spreading and retracting. Therefore, high receding contact angle and low contact angle hysteresis of a copolymer surface would be beneficial for the droplet retraction. Impacting droplet on **S-6F** surface at −20 °C underwent a significant increase in d_{min} due to its low receding contact angle and energy dissipation resulting from increased viscous shear of water droplet. For droplet impact on substrates at low temperature, the droplet dissipates more energy through the viscous effect during spreading and retracting process [41,42].

Fig. 9 displays the dynamic behavior of water droplets (7 μL) dropping on tilted (45°) copolymer surfaces at room temperature (or −20 °C). It showed that the d_{min} of sample **S-POSS-12F** at either room temperature or −20 °C was the smallest among all the samples. This result indicated that the supercooled water droplet would slip away from the tilted copolymer surface at −20 °C before it frozen.

3.5.2. Ice shear strength

Fig. 10 shows the ice shear strengths on fluorosilicone multi-block copolymer surfaces. The ice shear strengths on the copolymer films varied in range of 264–361 kPa. For comparison, the ice shear strength of commercial fluorinated polyurethane (F-PU) coating was also measured, with value of 691 ± 94 kPa. The ice shear strength of F-PU coating was significantly higher than those of block copolymer films due to the polar groups on F-PU surface, which would result in strong hydrogen bond between surface and ice. From Fig. 10, it can be seen that the ice shear strengths on **S-POSS** (272 ± 27 kPa), **S-POSS-6F** (264 ± 24 kPa) and **S-POSS-12F** (287 ± 18 kPa) surfaces were lower than those on **S-6F** (319 ± 24 kPa) and **S-12F** (361 ± 8 kPa), which could be associated with the incorporation of POSS block. The large POSS groups could prevent movement of polar groups to the surface, which would result in strong hydrogen bond between the surface and the ice. The fluorine percentages on **S-POSS**, **S-POSS-6F** and **S-POSS-12F** surfaces gradually increased from 0 wt% to 25.0 wt%. However, the ice shear strength values on the POSS-containing block copolymers were similar, suggesting that increasing fluorine content on the copolymer surface had little effect on reducing the ice shear strength. The low ice shear strength on the block copolymer surface is mainly attributed to the low T_g of PDMS block. The low T_g of PDMS chain infers the flexibility at low temperature and would result in dissimilar rheological–mechanical properties between ice and polymer surface, thereby leading to low ice shear strength [7–9]. Silicone-based polymers are found to perform better icephobicity than polyfluorocarbon (PFC)-based polymers [9]. Considering the XPS results, **S-POSS** and **S-POSS-6F** produced silicone-rich surfaces due to the high mobility of PDMS segments, which is beneficial for decreasing the ice shear strength. Because **S-POSS-12F** produced a fluorine-rich surface, the ice shear strength of **S-POSS-12F** was a little higher than those of **S-POSS** and **S-POSS-6F**. Though **S-POSS-12F** presented the best hydrophobicity among all the samples, the ice shear strength value of **S-POSS-12F** was not the lowest, suggesting that decreasing wettability of the block copolymer film did not have significant effect on reducing the ice shear strength. The ice shear strength on **S-6F** surface was lower than that on **S-12F**

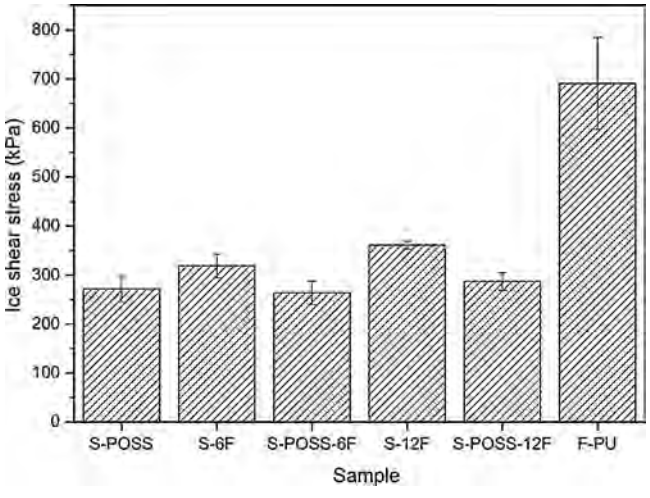

Fig. 10. Ice shear strength of the fluorosilicone multi-block copolymers films.

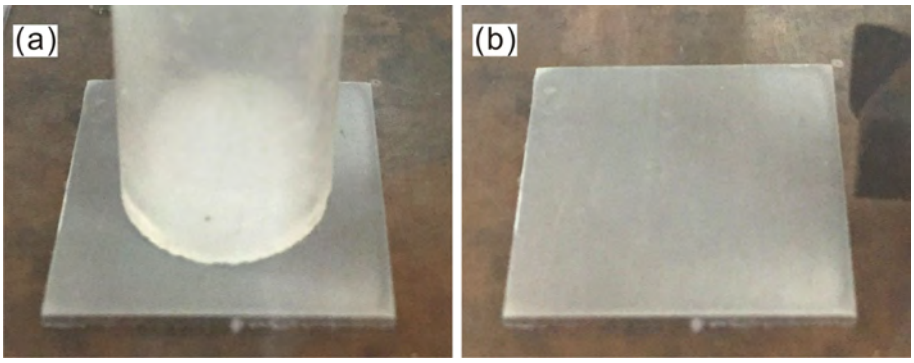

Fig. 11. Images of the **S-POSS-12F** surface before (a) and after (b) ice shear strength test.

surface, attributed to the higher content of the PDMS segments on **S-6F** surface, as compared with **S-12F**.

Meuler et al. found a strong correlation between ice adhesion strength and water wettability parameter ($1+\cos\theta_{rec}$, with θ_{rec} representing the receding contact angle) [43]. However, according to Ref. [8], the correlation is more appropriate for rigid substrates rather than for elastomeric substrates like Sylgard 184. In this study, the ice shear strengths on the copolymer film surfaces had little relationship with the receding contact angles perhaps due to the PDMS block which remains flexible at low temperature.

Moreover, as can be seen in Fig. 11, there was almost no ice residue left on **S-POSS-12F** surface after the ice shear strength test, indicating a loose ice structure at the interface between the ice block and the copolymer film surface. The nanostructure morphology of copolymer film presented a relatively smoother surface (Fig. 7), and the probable mechanical interlocking between ice and the copolymer surface was trivial. From icephobic tests, it can be assumed that decreasing wettability of the block copolymer film could minimize the surface accumulation of supercooled water.

4. Conclusions

POSS-containing fluorosilicone multi-block methacrylate copolymers PDMS-*b*-(PMAPOSS-*b*-PFMA)$_2$ were synthesized *via* RAFT polymerization using CTA-PDMS-CTA. The effect of different fluorinated side groups and PMAPOSS segments on the wettability and icephobic properties of copolymer films are discussed. The PDFHMA chains with longer fluorinated side groups, as compared with PHFBMA chains, were easy to migrate onto the surface. **S-POSS-12F** presented the biggest surface roughness (4.05 ± 0.07 nm), highest receding contact angle ($103.8\pm0.5^\circ$) and lowest water contact angle hysteresis ($8.7\pm1.4^\circ$) among all the samples due to the introduction of PMAPOSS and the synergistic effect of silicon and fluorine. Measurements of icephobic properties demonstrated that the supercooled water droplet could easily slip away from the tilted **S-POSS-12F** surface at $-20\,^\circ$C, ascribing to its high receding contact angle, and the reduction of ice shear strength was related to the incorporation of POSS block. Decreasing wettability of the block copolymer film could minimize the surface accumulation of supercooled water, but did not have significant effect on reducing the ice shear strength. The POSS-containing fluorosilicone block copolymers combine the advantages of PDMS, POSS and fluoropolymers, and could be a good candidate for icephobic applications.

Acknowledgments

This work is financially supported by National Natural Science Foundation of China (No. 51273146) and Natural Science Foundation of Tianjin, China (No. 14ZCZDGX00008).

References

[1] C.C. Ryerson, Cold Reg. Sci. Technol. 65 (2011) 97–110.
[2] N. Dalili, A. Edrisy, R. Carriveau, Renew. Sustain. Energy Rev. 13 (2009) 428–438.
[3] M. Susoff, K. Siegmann, C. Pfaffenroth, M. Hirayama, Appl. Surf. Sci. 182 (2013) 870–879.
[4] T. Bharathidasan, S.V. Kumar, M.S. Bobji, R.P.S. Chakradhar, B.J. Basu, Appl. Surf. Sci. 314 (2014) 241–250.
[5] R. Dou, J. Chen, Y. Zhang, X. Wang, D. Cui, Y. Song, L. Jiang, J. Wang, ACS Appl. Mater. Interfaces 6 (2014) 6998–7003.
[6] L. Zhu, J. Xue, Y. Wang, Q. Chen, J. Ding, Q. Wang, ACS Appl. Mater. Interfaces 5 (2013) 4053–4062.
[7] D.M. Yu, Y.H. Zhao, H. Li, H.Z. Qi, B. Li, X.Y. Yuan, Prog. Org. Coat. 76 (2013) 1435–1444.
[8] C. Wang, T. Fuller, W. Zhang, K.J. Wynne, Langmuir 30 (2014) 12819–12826.
[9] R. Menini, M. Farzaneh, J. Adhes. Sci. Technol. 25 (2011) 971–992.
[10] Z.H. Luo, T.Y. He, H.J. Yu, L. Dai, Macromol. React. Eng. 2 (2008) 398–406.
[11] J.Y. Liang, L. He, X. Zhao, X. Dong, H.J. Luo, W.D. Li, J. Mater. Chem. 21 (2011) 6934.
[12] C.M. Guan, Z.H. Luo, J.J. Qiu, P.P. Tang, Eur. Polym. J. 46 (2010) 1582–1593.
[13] T. Uragmi, H. Yamada, T. Miyata, Macromolecules 39 (2006) 1890–1897.
[14] H. Murase, K. Nanishi, H. Kogure, T. Fujibayashi, K. Tamura, N. Haruta, J. Appl. Polym. Sci. 54 (1994) 2051–2062.
[15] H. Murase, T. Fujibayashi, Prog. Org. Coat. 31 (1997) 97–104.
[16] S.A. Kulinich, S. Farhadi, K. Nose, X.W. Du, Langmuir 27 (2011) 25–29.
[17] S. Jung, M. Dorrestijn, D. Raps, A. Das, C.M. Megaridis, D. Poulikakos, Langmuir 27 (2011) 3059–3066.
[18] A.J. Meuler, G.H. McKinley, R.E. Cohen, ACS Nano 4 (2010) 7048–7052.
[19] H. Hussain, S.M. Shah, Polym. Int. 63 (2014) 835–847.
[20] W.A. Zhang, A.H.E. Müller, Prog. Polym. Sci. 38 (2013) 1121–1162.
[21] S. Yang, A. Pan, L. He, J. Colloid Interface Sci. 425 (2014) 5–11.
[22] A. Pan, S. Yang, L. He, X. Zhao, RSC Adv. 4 (2014) 27857.
[23] J. Wu, P.T. Mather, J. Macromol. Sci. C 49 (2009) 25–63.
[24] G. Moad, E. Rizzardo, S.H. Thang, Aust. J. Chem. 62 (2009) 1402–1472.
[25] X.H. Li, Y.H. Zhao, H. Li, X.Y. Yuan, Appl. Surf. Sci. 316 (2014) 222–231.
[26] B. Li, X.H. Li, K.Q. Zhang, H. Li, Y.H. Zhao, L.X. Ren, X.Y. Yuan, Prog. Org. Coat. 78 (2015) 188–199.
[27] C. Antonini, F. Villa, I. Bernagozzi, A. Amirfazli, M. Marengo, Langmuir 29 (2013) 16045–16050.
[28] P. Kim, T.-S. Wong, J. Alvarenga, M.J. Kreder, W.E. Adorno-Martinez, J. Aizenberg, ACS Nano 6 (2012) 6569–6577.
[29] Y. Mitsukami, M.S. Donovan, A.B. Lowe, C.L. McCormick, Macromolecules 34 (2001) 2248–2256.
[30] S. Boileau, L. Bouteiller, A. Kowalewsk, Polymer 44 (2003) 6449–6455.
[31] A.B. Orofino, M.F. Camezzana, M.J. Galante, P.A. Oyanguren, I.A. Zucchi, Nanotechnology 23 (2012) 115604.
[32] H. Fang, S. Zhou, L. Wu, Appl. Surf. Sci. 253 (2006) 2978–2983.
[33] H. Li, X.H. Li, C.H. Luo, Y.H. Zhao, X.Y. Yuan, Thin Solid Films 573 (2014) 73–76.
[34] M.L. Wadley, K.A. Cavicchi, J. Appl. Polym. Sci. 115 (2010) 635–640.
[35] X. Dong, L. He, N. Wang, J.Y. Liang, M.J. Niu, X. Zhao, J. Mater. Chem. 22 (2012) 23078–23090.
[36] M. Niu, L. He, J. Liang, A. Pan, X. Zhao, Prog. Org. Coat. 77 (2014) 1603–1612.
[37] R. Chen, W. Feng, S. Zhu, G. Botton, B. Ong, Y. Wu, Polymer 47 (2006) 1119–1123.
[38] Y.Y. Wang, J. Xue, Q.J. Wang, Q.M. Chen, J.F. Ding, ACS Appl. Mater. Interfaces 5 (2013) 3370–3381.
[39] V. Bahadur, L. Mishchenko, B. Hatton, J.A. Taylor, J. Aizenberg, T. Krupenkin, Langmuir 27 (2011) 14143–14150.
[40] Y.H. Yeong, J. Burton, E. Loth, Langmuir 30 (2014) 12027–12038.
[41] K.R. Khedir, G.K. Kannarpady, H. Ishihara, J. Woo, M.P. Asar, C. Ryerson, A.S. Biris, Appl. Surf. Sci. 279 (2013) 76–84.
[42] L. Mishchenko, B. Hatton, V. Bahadur, J. Taylor, T. Krupenkin, J. Aizenberg, ACS Nano 4 (2010) 7699–7707.
[43] A.J. Meuler, J.D. Smith, K.K. Varanasi, J.M. Mabry, G.H. Mckinley, R.E. Cohen, ACS Appl. Mater. Interfaces 2 (2010) 3100–3110.